https://doi.org/10.5194/egusphere-2026-5130
Preprint. Discussion started: 14 September 2026

The drag-law for turbulent air-sea interaction is locally linear

Achim Wirth
Univ. Grenoble Alpes, CNRS, LEGI, F-38000 Grenoble, France
Correspondence: Achim Wirth (achim.wirth@legi.cnrs.fr)

Abstract. The momentum transfer between the atmosphere and the ocean is typically parameterized using a quadratic drag law. However, analytical calculations reveal that such a drag law leads to a vorticity blow-up. Results from dedicated numerical simulations demonstrate that, at horizontal scales several times the boundary layer thickness, the drag parameterization is locally linear.

1 Introduction

The exchange of momentum, heat, water, and chemical fluxes at the atmosphere-ocean interface is fundamental to the dynamics of the atmosphere, ocean, and climate, as well as their responses to changes in climate forcing (Stocker et al. (2013); Csanady (2001)). These interfacial fluxes arise from a wide array of physical processes operating across a vast range of spatial and temporal scales—from the molecular dynamics of spray (Veron (2015)), to waves (with wavelengths from millimeters to hundreds of meters), to wave breaking (Melville (1996)), sub-mesoscale fronts (Small et al. (2008)), synoptic-scale cyclones (Emanuel (1986)), basin-scale phenomena (Bjerknes (1964)), and global patterns (Alexander et al. (2002); Van Westen et al. (2024)). These processes are inherently non-linear and interact in complex ways.

A fundamental aspect of the interaction is the stark contrast in density between water and air, with water being approximately 800 times denser than air. This disparity not only affects other physical properties such as heat capacity and viscosity but also influences the characteristic spatial and temporal scales of the dynamics. As a result, a stiffness problem arises in both space and time, making it challenging to perform calculations that accurately capture the small (O(1 km)) submeso-scale ocean dynamics, the large synoptic dynamics in the atmosphere (O(1000 km)) in space, and the fast submeso-scale dynamics in the atmosphere (O(1h)), the slow synoptic-scale dynamics in the ocean (O(1 month)) in time. The simulation of the atmosphere-ocean system relies therefore on the fidelity of the parameterizations and the precision of the corresponding parameter values. The former are derived with the help of first principles, while the latter are mostly empirical.

The parameterizations are called bulk formulas (Kondo (1975); Fairall et al. (1996); Castellari et al. (1998); Pelletier et al. (2021)), they approximate the effects of unresolved dynamics on the resolved scales in simulations of atmospheric, oceanic, and climate systems.

In this paper, I focus exclusively on the exchange of momentum, which is driven by shear stress. This shear depends not only on atmospheric wind but also on a variety of other physical factors, including ocean velocity, sea state, and density stratification in both the atmosphere and the ocean. When the friction force of a turbulent flow over a rough surface is estimated based on

https://doi.org/10.5194/egusphere-2026-5130
Preprint. Discussion started: 14 September 2026

the flow velocity at some distance, the prominent quadratic drag-law (given in Eq. 2) is commonly employed and found to provide an excellent parameterization (see Schlichting and Gersten (2016) for a general discussion and Deardorff (1972) for the atmospheric boundary layer).

While the quadratic drag law is fundamental in engineering fluid dynamics for calculating drag forces of turbulent flow in pipes or over rough surfaces, it cannot be directly applied as a bulk formula for air-sea interactions at horizontal scales much larger than the thickness of the three-dimensional atmospheric or oceanic boundary layer. Indeed, the quadratic drag-law is meant to parameterize the effect of the small-scale three-dimensional boundary-layer turbulence but is not adapted to also handle the two-dimensional, larger-scale, boundary-layer turbulence in the atmosphere and the ocean. Another important aspect is the lack of scale separation of the horizontal dynamics, between the explicitly resolved large-scale and the smaller sub-grid-scale (SGS) scale of turbulence generated by instability. Specifically, because of the inverse energy cascade in two-dimensional turbulence (Boffetta and Ecke (2012)), the size of turbulent structures continues to grow, only limited by bottom drag, and can exceed the original forcing scale.

In the next section, I demonstrate that the quadratic drag-law is ill defined, resulting in a vorticity blow-up. In the same section, I discuss a standard bulk-formula that combines the quadratic drag law with a linear Rayleigh friction. A numerical model consisting of two superposed quasigeostrophic layers, the upper representing the atmosphere and the lower representing the ocean, is introduced in Section 3. In Section 4, the averaged results from the numerically integrated model will be used to determine the bulk friction-law, which is shown to be predominantly locally linear. The consequences of the findings presented here for a bulk formula of air-sea interaction are discussed in Section 5.

2 Theory

The viscous drag exerted by a flow on a solid boundary depends linearly on the velocity-gradient normal (z-direction) to the boundary ($z = 0$):

$$\tau = \nu \partial_z \mathbf{u}(0), \tag{1}$$

where ν is the viscosity. At high Reynolds number the flow is turbulent and its details can, in most applications, not be resolved in measurement and numerical simulation. When an average flow velocity $\mathbf{u}$ at some distance, l, within the turbulent boundary layer but beyond the laminar friction layer, is considered, the magnitude of the drag-force is proportional to the square of this velocity, leading to the prominent quadratic drag-law (see Schlichting and Gersten (2016)) for the shear,

$$\tau = c\rho\sqrt{\mathbf{u}^2}\ \mathbf{u}, \tag{2}$$

where ρ is the density of the fluid, the vector $\mathbf{u}$ represents the velocity at some distance l from the interface, outside the viscous sub-layer. The value of the drag coefficient c is a function of this distance and depends on the roughness of the surface. This frictional law parameterizes the effect of three dimensional boundary layer turbulence.

When the drag between the atmosphere and the ocean is considered a large number of physical processes from the molecular scale (molecular drag, spray and bubble formation and evaporation) to the wave scale (wave formation, evolution and

https://doi.org/10.5194/egusphere-2026-5130
Preprint. Discussion started: 14 September 2026

breaking) to the sub-synoptic scale (Ekman dynamics, Langmuire dynamics, convection, frontal dynamics and the associated instabilities) to the synoptic scale (two dimensional turbulence) are important. These processes will not be explicitly resolvable in calculations of climate dynamics in a foreseeable future and their effect on the explicitly resolved, larger-scale dynamics, has to be parameterized. In the case of air-sea interaction, the sea surface is not flat and moves in time due to waves and a pressure drag adds to the drag force (Melville (1996), Wu et al. (2024)). When waves brake ocean spray is created which also adds to the momentum exchange between the atmosphere and the ocean Veron (2015). In the case of air-sea interaction, the vector $\mathbf{u}(l_a, l_o)$ represents the velocity difference between the atmospheric wind at some distance l_a and the ocean current at some distance l_o from the interface and the value of the coefficient $c(l_a, l_o)$ is a function of these distances.

Equation 2 appears in the beginning of mostly every paper or chapter on the momentum exchange at the atmosphere-ocean interface. The problem with the quadratic drag law is that it is often used to parameterize not only the unresolved three-dimensional turbulent boundary-layer dynamics (O(10^{-3} – 10^2 m) in the atmosphere and O(10^{-3} – 10^1 m) in the ocean), but also the smaller part of the two-dimensional turbulent dynamics (O(10^2 m) – O(10^5 m)) that is not explicitly resolved. I argue that to include the two dimensional turbulence the above quadratic law has to be extended to:

$$\tau = \sqrt{(c\mathbf{u})^2 + a^2}\ \mathbf{u}, \tag{3}$$

where a^2 represents the unresolved two-dimensional sub-grid-scale (SGS) dynamics, and $u = a/c$ can be interpreted as a SGS speed. For vanishing values of a^2 the drag law is quadratic and Eq. 2 is recovered. While for larger values of a^2, as compared to the resolved drag $(c\mathbf{u})^2$, the law approaches linear Rayleigh drag. The inclusion of a linear term is already used in air-sea interaction studies (see, for example, Pelletier et al. (2021) and Stevens et al. (2002)). In the former, the linear term is introduced to account for molecular effects and to ensure the parameterization remains valid down to and up to the interface. In the latter, it is used to parameterize entrainment fluxes at the top of the atmospheric boundary layer. Furthermore, measurements of the drag coefficient are found to diverge with decreasing wind-speed under low-wind conditions pointing to a sub-quadratic drag-law Wei et al. (2016).

Note also that when it comes to bottom drag a linear wave-drag term is often added (see e.g. Wirth (2011); Buijsman et al. (2016) for the ocean and Lott et al. (2026) for the atmosphere) and linear bottom drag was employed in early simulations of ocean dynamics (see Pond and Bryan (1976)). Drag laws combining linear and quadratic drag are typically implemented to parameterize bottom drag in ocean models (as in the Hycom model https://www.hycom.org, where typically, a residual velocity of 0.1 m s^{-1} is added to the resolved velocity). See also Arbic and Scott (2008) for a comparison of quasi-geostrophic two-layer simulations with a linear and a quadratic bottom drag.

I here argue that Eq. 2 is unfit as a bulk formula for air-sea interaction because: firstly, it leads to a divergence of the vorticity and, secondly, numerical evidence clearly points to a dominance of linear drag over the quadratic law (to be shown in Section 4). Concerning the first point, it was already shown in Moulin and Wirth (2014) that when the flow is subject to a transverse sine-forcing, with the components $F_x = 0$, $F_y = F_0 \sin(2\pi x)$, the stationary laminar solution of of the quadratic drag-law (Eq. 2) :

$$0 = -c\sqrt{\mathbf{u}^2}\ \mathbf{u} + \mathbf{F}, \tag{4}$$

https://doi.org/10.5194/egusphere-2026-5130
Preprint. Discussion started: 14 September 2026

is:

$$u(x) = 0 \quad \text{and} \quad v(x) = \text{sign}(\sin(x))\sqrt{\sin(x)/c} \tag{5}$$

where "sign" is the signum function. This leads to a vorticity of

$$\zeta(x) = \text{sign}(\sin(x))\frac{\pi\cos(x)}{\sqrt{c\sin(x)}} \tag{6}$$

which diverges at $x = n\pi$, with $n \in \mathbb{Z}$. The divergence is avoided by the extended drag-law (Eq. 3) with a non vanishing a^2. The extended drag-law is, therefore, not only a representation of the two-dimensional SGS dynamics but also imposes itself to assure a well definedness of the vortical dynamics.

3 The model

To investigate the drag law governing air-sea interactions, an idealized model is developed. The physical context is addressed in the following subsection. For the mathematical framework, the quasi-geostrophic equations are adopted (see Subsection 3.2), while a spectral model is implemented for numerical simulations (see Subsection 3.3). All these models are standard in the context of geophysical fluid dynamics.

3.1 The physical model

The physical situation consists in an atmospheric layer subject to a large scale forcing (large as compared to the thickness of the layer) superposing an oceanic layer. The interaction is through drag between the two layers leading to a momentum exchange. The system is evolving in a rotating frame.

The physical parameters, all given in Table 1, are the thicknesses of the atmospheric and the oceanic layer, (h_a, h_o), the mass ratio of the oceanic and atmospheric layer (m) and the Coriolis parameter (f). Two horizontal length scales, the atmospheric (R_a) and oceanic (R_o) Rossby radii of deformation $(R = \sqrt{g'h/f})$, can be derived and compared to the forcing length-scale (R_F). The momentum exchange is governed by the drag coefficient (c_d) between the atmosphere and the ocean and the characteristic atmospheric velocity (u_a) induced by the forcing strength (F_a). The ratio $\frac{R_F}{R_a} = 1$, measuring the forcing scale to the synoptic scale, is smaller than in reality, this is imposed by constraints on numerical resolution. The ratio of the synoptic scale of the atmosphere and the ocean $\frac{R_a}{R_o} = 5$, this corresponds roughly to mid-latitude dynamics. Indeed, on our planet we typically have $R_F \approx 4\cdot 10^6 m$, $R_a \approx 10^6 m$, $R_o \approx 10^5 m$. No clear scaling laws can be obtained as the ratios between the different scales are insufficient.

The equations are put into a mathematical form by non-dimensionalization. The non-dimensional atmospheric drag strength parameter $\tilde{c} = \frac{c_d R_a}{h_a}$ (Arbic and Scott (2008)) compares advection to the drag and the Reynolds number $(Re = \nu_a/(R_a u_a))$ compares advection to internal, viscous dissipation. It is interesting to note that the parameter equals unity, that is, advective time equals the drag time, meaning that the wind (u_a) at the synoptic scale will decay at the same time $t_a = c_d R_a/h_a$ that it takes an air parcel to traverse the same scale $t_a = R_a/u_a$, showing that the system is a forced and damped system. The

https://doi.org/10.5194/egusphere-2026-5130
Preprint. Discussion started: 14 September 2026

Table 1. Physical parameters and non-dimensional equivalent. Subscript $._a$ stands for the atmospheric value and $._o$ for the oceanic value.

name	**symbol**	**value** (dim)	**value** (adim)
Horizontal extension	L	$2 \cdot 10^6$ m	4
Rossby radius atmosphere	R_a	$5 \cdot 10^5$ m	1
Rossby radius ocean	R_o	$1 \cdot 10^5$ m	1/5
forcing scale	R_F	$5 \cdot 10^5$ m	1
atmospheric layer thickness	h_a	800 m	
oceanic layer thickness	h_o	50 m	
mass ratio ocean / atmos	$m = \frac{\rho_o h_o}{\rho_a h_a}$		50
drag strength parameter	c_d	$1.6 \cdot 10^{-3}$	
drag strength parameter	$\tilde{c} = \frac{c_d R_a}{h_a}$		1.
wind speed	u_a	10 m s^{-1}	1
wind vorticity	ζ_a	$2\pi 10^{-5}$ s^{-1}	2π
advective time scale	$t_a = R_a/u_a$	$5 \cdot 10^4$ s	1
drag time scale	$t_a = \frac{h_a}{c_d u_a}$	$5 \cdot 10^4$ s	1

dimensional and adimensional values are given in Table 1, symbols are overloaded as they stand for the dimensional and adimensional variable, no confusion is possible. From hereon all parameters are non-dimensional.

3.2 The mathematical model

The appropriate mathematical model to investigate the dynamics around and above the synoptic scale, is the quasi-geostrophic model (see Vallis (2017)). Its divergenceless velocity field is expressed by a stream function through:

$$u = -\partial_y \Psi \tag{7}$$

$$v = \partial_x \Psi \tag{8}$$

and the potential vorticity by:

$$q = \nabla^2 \Psi - R^{-2} \Psi \tag{9}$$

In Fourier space we see that:

$$\hat{\zeta} = -\mathbf{k}^2 \hat{\Psi} \tag{10}$$

$$\hat{q} = -(\mathbf{k}^2 + k_R^2)\hat{\Psi} = (1 + \frac{k_R^2}{\mathbf{k}^2}),\hat{\zeta} \tag{11}$$

where the hat symbol $\hat{q}(\mathbf{k})$ denotes the two-dimensional Fourier-transform of the variable $q(x,y)$ depending on the wave-vector $\mathbf{k} = (k_x, k_y)$. The quasi-geostrophic equations for the atmospheric (subscript $._a$) and oceanic (subscript $._o$) layer, interacting

https://doi.org/10.5194/egusphere-2026-5130
Preprint. Discussion started: 14 September 2026

through drag at the interface, are given by:

$$\partial_t q_a \quad + \mathcal{J}(\Psi_a, q_a) = \frac{c_d}{h_a} \quad \mathcal{A}(\Psi_a - \Psi_o) + \nu_a \nabla^2 q_a + \tilde{\nu_a} (\nabla^2)^5 q_a + F \tag{12}$$

$$\partial_t q_o \quad + \mathcal{J}(\Psi_o, q_o) = \frac{c_d}{h_a m} \quad \mathcal{A}(\Psi_o - \Psi_a) + \nu_o \nabla^2 q_o + \tilde{\nu_o} (\nabla^2)^5 q_o. \tag{13}$$

where the Jacobian operator is defined as:

$$\mathcal{J}(f,g) = (\partial_x f)(\partial_y g) - (\partial_x g)(\partial_y f), \tag{14}$$

m is the mass ratio between the oceanic and the atmospheric layer. The variable F represents the forcing applied to the atmosphere. It represents the action of a horizontal pressure-gradient due to density differences or the dynamics of layers superposing the atmospheric boundary layer. The Rossby radii in the atmosphere and the ocean differ. The air-sea interaction operator is defined as:

$$\mathcal{A}(\Psi) = \partial_y (U \partial_y \Psi) + \partial_x (U \partial_x \Psi), \qquad \text{with} \qquad U = \sqrt{(\partial_y \Psi)^2 + (\partial_x \Psi)^2 + \bar{v}^2}. \tag{15}$$

The atmospheric drag coefficient at the air-sea interface is c_d. The model is purely two-dimensional and the veering of the velocity vector due to Ekman-dynamics near the interface is neglected. The viscosity in the layers are ν_a, ν_o and its value depends on the numerical resolution of the integration (see Subsection 3.3). The same applies to the non-physical hyper-dissipation fifth-power operator with hyper-viscosities $\tilde{\nu_a}, \tilde{\nu_o}$, it is added to damp the smallest scales in the dynamics and assures numerical stability by preventing a pile-up of enstrophy at the smallest-scales.

We next put the equation in non-dimensional form. We first non-dimensionalize the horizontal scale by the atmospheric Rossby-radius R_a and the velocity by u_0. Potential vorticity is non-dimensionalized by $q_0 = u_0/R_a$ time by q_0^{-1} and the stream function by $\Psi_0 = u_0 R_a$. The key parameter is the non-dimensional drag strength (Arbic and Scott (2008)) that compares advection to interfacial drag is $\tilde{C} = \frac{c_d R_a}{h_a}$, the Reynolds number is $Re = u_0 R_a / \nu$. Typical values are $R_a = 10^6$ m, $h_a = 10^5$ m leading to $\tilde{C} = 1$.

3.3 The numerical model

For the numerical implementation a horizontal two-dimensional pseudo-spectral code, based on Fourier-series, is used for the atmosphere and the ocean. The horizontal boundary conditions are periodic. The resolution is $n_x = n_y = 1024$ grid points, in the atmosphere and the ocean. The viscosity values are chosen such that structures are resolved with more than ten grid-points. The time stepping is performed by a third-order low-storage Runge-Kutta scheme with a CFL-condition which is always below 0.2. Such conservative values for resolution and CFL-condition are appropriate in a pioneering simulation, with no possibility to validate the results with observation laboratory experiments or other numerical results. The viscosity in the atmosphere and the ocean depends on the numerical resolution and the numerical viscosity of the scheme used. It is there to dissipated the enstrophy at the smallest scales and is therefore a numerical parameter. The numerical values are given in Table 2. The same applies to the fifth-order Laplace-operator its numerical value is chosen that the dissipation equals the viscous dissipation at the scale three-times the Laplace distribution.

https://doi.org/10.5194/egusphere-2026-5130
Preprint. Discussion started: 14 September 2026

Table 2. Numerical parameters: horizontal viscosity in the atmosphere ν_a and the ocean ν_o :

experiment	ν_a	ν_o
N311000	$2 \cdot 10^{-4}$	$4 \cdot 10^{-5}$
N311001	$2 \cdot 10^{-4}$	$4 \cdot 10^{-5}$
N311002	$5 \cdot 10^{-6}$	$1 \cdot 10^{-6}$
N311100	$2 \cdot 10^{-4}$	$2 \cdot 10^{-5}$
N311101	$2 \cdot 10^{-4}$	$2 \cdot 10^{-5}$
N311200	$4.5 \cdot 10^{-4}$	$2 \cdot 10^{-5}$
N311201	$4.5 \cdot 10^{-4}$	$2 \cdot 10^{-5}$
N311300	$2.5 \cdot 10^{-4}$	$1 \cdot 10^{-5}$
N311301	$2.5 \cdot 10^{-4}$	$1 \cdot 10^{-5}$
N311302	$5 \cdot 10^{-9}$	$1 \cdot 10^{-10}$

For all the two-dimensional calculation a one-dimensional calculation was performed with the same viscosity parameters to evaluate the effect of the explicit viscosity and for two experiments one dimensional calculation with strongly reduced viscosity-parameters were performed to verify that the analytic results were recovered (see Table 3)

3.4 Averages

The forcing F has periodicity R_F in the x-direction with $p = L/R_F = 4$ and it does not depend on the y-direction. Quantities taken at a distance R_F in the x-direction and different y are statistically equivalent and can be averaged over. We denote averaging over the forcing symmetries by $\langle . \rangle_F$. Such average depends on $x = [0,1[$, only. In the discretized numerical grid with (n_x, n_y) points, the average $\langle . \rangle_F$ is given by:

$$\langle a \rangle_F(\bar{i}) = \frac{1}{pn_y} \sum_{i=0,p-1;j=1,n_y} a(ip + \bar{i}, j), \tag{16}$$

where $\bar{n}_x = n_x/p$ and $\bar{i} = 1, \ldots, \bar{n}_x$. Note that the quasi-geostrophic model has also the symmetry: $\langle a \rangle_F(\bar{i}) = -\langle a \rangle_F(\bar{i} + n_x/2)$ for $\bar{i} = 1, \ldots, \bar{n}_x/2$, for variables depending linearly on the vorticity.

3.5 Non Stationary States

In the results discussed here, the dynamics are in a non-equilibrium, non-stationary state, as the constant forcing leads to an increase in energy and enstrophy in both the atmosphere and ocean. After a very long time $t^{total}_{\mathrm{stat}}$, the dynamics may reach a stationary non-equilibrium state when the forcing is balanced by dissipation in the atmosphere, the ocean and a the interface. Such state is not reached in neither of the experiments presented here. Moreover, if in the ocean the horizontal eddy viscosity is negligible compared to the atmospheric forcing, which both injects and drains energy from the ocean, the ocean may approach a stationary equilibrium state.

https://doi.org/10.5194/egusphere-2026-5130
Preprint. Discussion started: 14 September 2026

More precisely, when the system starts from rest the atmosphere accelerates and is damped at a characteristic time scale of $h_a/(c\bar{v})$. The drag accelerates the ocean which responds at a characteristic time scale of $h_a m/(c\bar{v})$. The regime we are exploring here is that after this initial adjustment. In this regime the energy in the atmosphere and the ocean continues to increase but the shear velocity between the atmosphere and the ocean,

$$u_s = u_a - u_o \text{ and } v_s = v_a - v_o \qquad (17)$$

reaches a statistically stationary state (see Moulin and Wirth (2016); Wirth (2018, 2019)), this timescale is called $t_{\rm stat}^{\rm shear}$. In the laminar case it is equal to $\tilde{t}_C$ Note that the same is not true for the potential vorticity, that is $q_a - q_o$ reaches a stationary state only after the very long time scale $t_{\rm stat}^{\rm total}$, as the Rossby radii differ (see Appendix A). This time scale depends on the horizontal viscosities in the atmosphere and the ocean.

4 Results

Experiments were performed for four different drag coefficients forming a geometric series with a common ratio of 2. For each of these values two-dimensional and one-dimensional simulations where performed. The former gave rise to instability and eddy dynamics in the ocean and the atmosphere, whereas the latter is constraint to laminar motion and allows for comparison to analytic solutions and to assure that the discretisation error is negligible. The two-dimensional experiments start from a slightly perturbed initial condition, forcing strength is $\hat{F} = 1$ and the integration time is $t = 3000$ in all experiments.

Table 3. Initial and turbulent drag coefficients:

experiment	c^2	a^2	$\bar{c}^2$	$\bar{a}^2$	d	nl
N311000	4	$4{\cdot}10^{-1}$	1.16	3.01	$4.06{\cdot}10^{-3}$	$1.04{\cdot}10^{-1}$
N311001	4	$4{\cdot}10^{-1}$	4.04	$4.40{\cdot}10^{-1}$	$1.03{\cdot}10^{-2}$	$8.04{\cdot}10^{-1}$
N311002	4	$4{\cdot}10^{-1}$	4.01	$4.01\ {\cdot}10^{-1}$	$5.4{\cdot}10^{-4}$	$8.18{\cdot}10^{-1}$
N311100	1	$1{\cdot}10^{-1}$	$4.8\ {\cdot}10^{-1}$	2.65	$2.33{\cdot}10^{-2}$	$6.52{\cdot}10^{-2}$
N311101	1	$1{\cdot}10^{-1}$	1.01	$1.25{\cdot}10^{-1}$	$1.78{\cdot}10^{-2}$	$8.84{\cdot}10^{-1}$
N311200	$2.5\ {\cdot}10^{-1}$	$2.5{\cdot}10^{-2}$	$1.5\ {\cdot}10^{-1}$	3.75	$6.48{\cdot}10^{-2}$	$3.44{\cdot}10^{-2}$
N311201	$2.5\ {\cdot}10^{-1}$	$2.5{\cdot}10^{-2}$	$2.52\ {\cdot}10^{-1}$	$3.32{\cdot}10^{-2}$	$1.93{\cdot}10^{-2}$	$9.36{\cdot}10^{-1}$
N311300	$6.25\ {\cdot}10^{-2}$	$6.25{\cdot}10^{-3}$	$6.5\ {\cdot}10^{-1}$	4.76	$1.16{\cdot}10^{-1}$	$5.55{\cdot}10^{-2}$
N311301	$6.25\ {\cdot}10^{-2}$	$6.25{\cdot}10^{-3}$	$6.29\ {\cdot}10^{-2}$	$2.45{\cdot}10^{-2}$	$2.27{\cdot}10^{-2}$	$9.05{\cdot}10^{-1}$
N311302	$6.25\ {\cdot}10^{-2}$	$6.25{\cdot}10^{-3}$	$6.26\ {\cdot}10^{-2}$	$6.25{\cdot}10^{-3}$	$2.0{\cdot}10^{-4}$	$9.75{\cdot}10^{-1}$

The potential vorticity in the atmosphere and the ocean at $t = 1000$ is given in Fig. 1 for experiments exp 311000 and exp311300. The first shows a close to periodic structure, the periodicity will slowly fade in time, while the second shows a disordered eddy dynamics already at $t = 1000$.

https://doi.org/10.5194/egusphere-2026-5130
Preprint. Discussion started: 14 September 2026

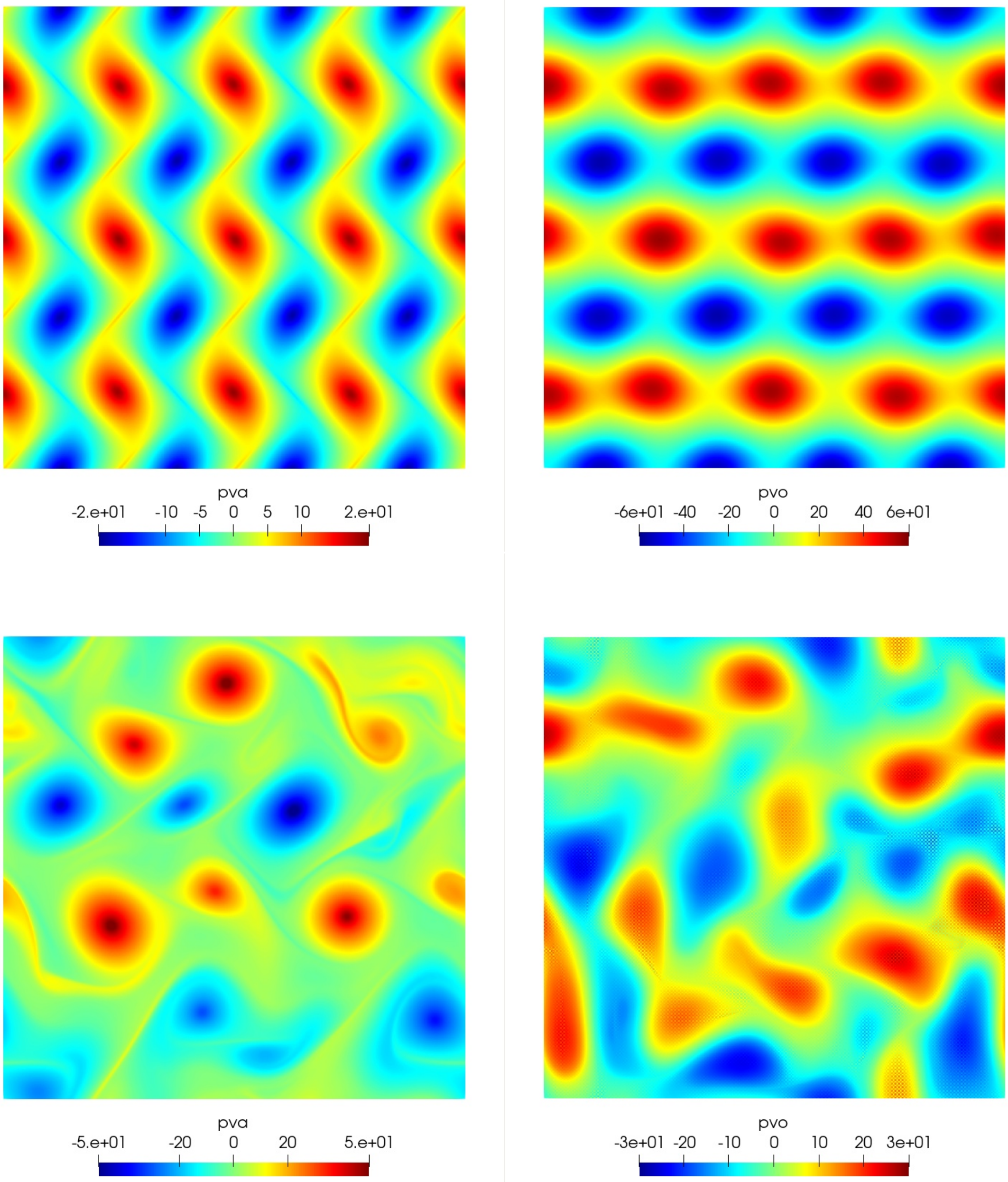

Figure 1. Color plots of potential vorticity at $t = 1000$ of exp311000 (upper panels) and exp311300 (lower panels) of the atmosphere (left panels) and the ocean (right panels).

https://doi.org/10.5194/egusphere-2026-5130
Preprint. Discussion started: 14 September 2026

The purpose of this work is to determine to what extend the bulk drag is linear or quadratic. The basis of the argumentation is Eq. 3. To this end, the averaged shear velocity ($\tilde{v} = \langle v_a - v_o \rangle_F$) is measured from the numerical experiment data and presented in Fig. 2, for the different experiments. While the laminar cases show a shape close to Eq. 5, the eddying 2D simulations exhibit a shape close to a sine wave, which points towards a linear drag-law. The quantitative analysis to discriminate between the two behaviors is based on Eq. 3 and detailed in Appendix A. It compares the maximum at $x = 1/4$ minus the minimum at $x = 3/4$, to the difference of the second derivatives at the same locations. The second derivative, normalized by the amplitude, at these points is reduced when the quadratic component in the drag is augmented. Using the formalism from Appendix A the eddy drag-coefficients $\bar{c}^2$ and $\bar{a}^2$ are calculated and presented in Fig. 3 as a function of time. The values of $\bar{c}^2$ and $\bar{v}^2$ averaged over time, from $t = 300$, when initial adjustment has resided in all experiments, to $t = 3000$ ($t = 1000$, for the non-turbulent experiments) are given in Table 3. These eddy drag-coefficients are then used to reconstruct the shape of the shear velocities ($\tilde{v}_R$), which is then compared to the measured averaged shear velocities ($\tilde{v}$) from the simulations. Results presented in Fig. 2 show that the reconstruction coincides well with the measurement, giving credit to the drag law of Eq. 3. For a qualitative analysis the difference,

$$d = \sqrt{\frac{(\hat{v} - \hat{v}_R)^2}{\hat{v}^2}}, \tag{18}$$

is evaluated in Figs. 4. where $\hat{v} = (\tilde{v}(1/4) - \tilde{v}(3/4))/2$ is the maximum of the average shear velocity.

To show that the drag is linear rather than quadratic the criteria,

$$nl = \sqrt{\frac{(\bar{c}\hat{v})^2}{(\bar{c}\hat{v})^2 + a^2}}, \tag{19}$$

is used. The variable is unity for purely quadratic drag and vanishes for linear drag. Its time evolution is presented in Fig. 5 and the time averages are given in Table 3. Results clearly show that the linear drag dominates in the 2D experiments, while for the 1D experiments the variable nl is imposed by the parameters of the experiments.

Two laminar experiments for two different drag values (exps. 3110001, 3110002, 3113001, 3113002), one with horizontal viscosities from the eddying simulations and one with a strongly reduced viscosity values, were performed. The purpose is two-fold, first to verify that for the low viscosity values the results compare very well to the imposed drag parameters, thereby validating the estimation procedure of Appendix A, and second, evaluating that the explicit influence of the horizontal viscosities does not significantly modify the estimated drag parameters.

It can be seen that the quadratic drag coefficient is not always well defined, when $\bar{c}^2 < 0$. This occurs when the second derivative at the maximum values is larger than those of a sine function with the same amplitude. For the most turbulent cases it also shows a strong variability, as the domain is not large enough to self-average.

5 Discussion and Conclusions

In models with a horizontal resolution coarser than the layer thickness the drag law not only parameterizes the three-dimensional boundary-layer turbulence but also the SGS part of the two-dimensional dynamics. The here presented results demonstrate that

https://doi.org/10.5194/egusphere-2026-5130
Preprint. Discussion started: 14 September 2026

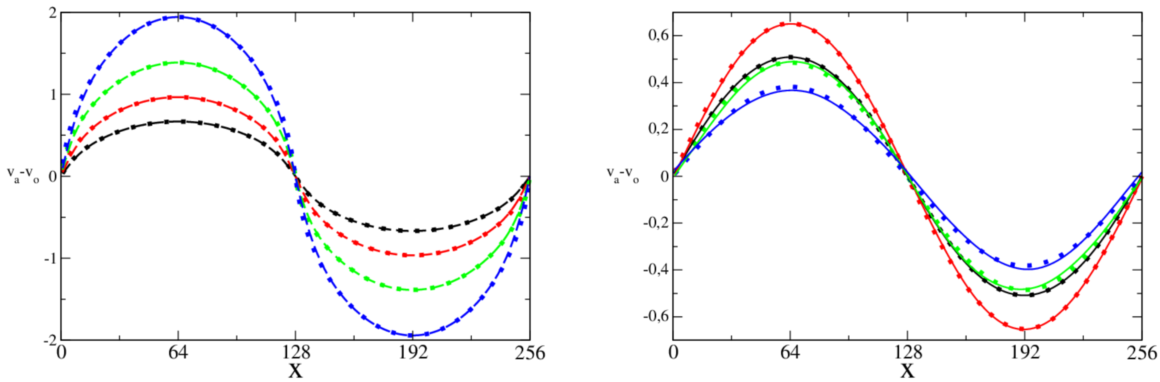

Figure 2. Comparison of the reconstructed analytic-solution (v_R, dotted lines) based on the measured parameters $\bar{c}^2$ and $\bar{v}^2$ to the shape of the averaged velocity profile ($\langle v \rangle_F$ dashed (left) and continuous (right) line) for a snapshot ($t = 1000$). The non-turbulent experiments in the left panel (exp 311001 black, exp 311101 red, exp 311201 green, exp 311301 blue) show a clear signature of the quadratic drag-law (see Eq. 5), while on the right panel the turbulent experiments (exp 311000 black, exp 311100 red, exp 311200 green, exp 311300 blue) exhibit shapes that correspond closely to the sine shape of a linear drag-law.

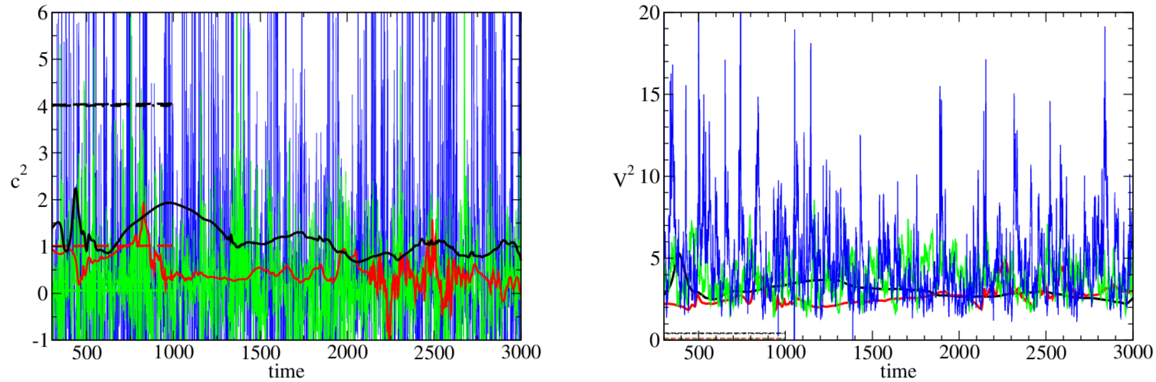

Figure 3. Diagnosed values of $\bar{c}^2$ and $\bar{a}^2$ for the analyzing period ($t = 300$–1000 for the 1D simulations, showing negligible variability, and $t = 300$–3000 for the 2D simulations). Continuous lines are for the 2D experiments and dashed lines for 1D experiments. exp 311000 continuous black line, exp 311001 dashed black line, exp 311002 dashed-dotted black line, exp 311100 continuous red line, exp 311101 dashed red line, exp 311200 continuous green line, exp 311201 dashed green line, exp 311300 continuous blue line, exp 311301 dashed blue line. Average values are given in Tab. 3.

https://doi.org/10.5194/egusphere-2026-5130
Preprint. Discussion started: 14 September 2026

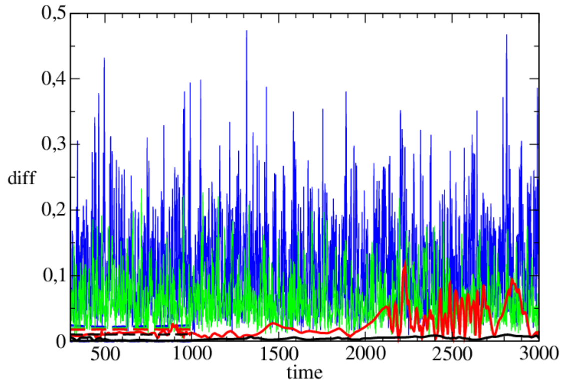

Figure 4. The differences between the reconstructed analytic solution with the measured parameters $\bar{c}^2$ and $\bar{v}^2$ to the shape of the averaged velocity profile, based on Eq. 18 over the analyzing period. Average values are given in Tab. 3.

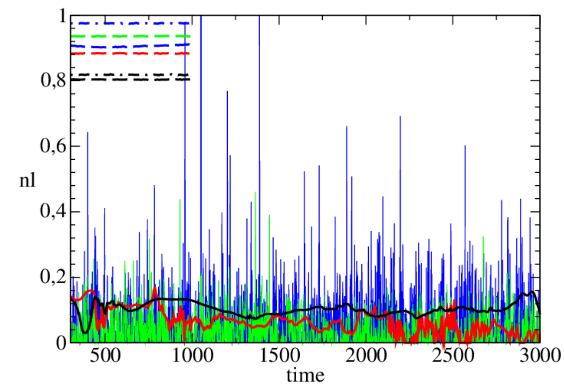

Figure 5. The non-linearity index nl from Eq. 19 shows that the drag in the turbulent simulations is close to linear. While it has the value imposed by the predefined parameters in the non-turbulent simulations. Average values are given in Tab. 3.

https://doi.org/10.5194/egusphere-2026-5130
Preprint. Discussion started: 14 September 2026

a locally linear rather than a quadratic drag-law has to be employed. Indeed, while the non-turbulent simulations yield the drag parameters chosen prior to the simulation, with a dominant quadratic term, the linear drag dominates in all turbulent simulations. By "locally linear" I propose a drag law of the form:

$$\tau = C_{2D}\left(\sqrt{\langle \mathbf{u_s^2} \rangle}\right)\ \mathbf{u_s}. \tag{20}$$

In this formulation the drag depends linearly on the local value of the shear velocity, while the coefficient depends non-locally on the average of the shear speed. That is, for the present case the variables c and a in Eq. 3 are functions of the average of the shear speed. The function, C_{2D} can be linear, resulting in a non-local quadratic drag-law, or not. The dependence is non-local as it involves an average, rather than the local value. The non-locality resolves also the problem of the blow-up in the vorticity exposed in Moulin and Wirth (2014) and which is revisited in the Section 2. In the case of rotating two-dimensional turbulence with an inverse energy cascade, the non-locality is amplified as the sub-grid-scale energy does not cascade to smaller scales where it is dissipated. Instead, it cascades to larger scales, further affecting the resolved dynamics (Boffetta and Ecke (2012).

I determined that the drag law is locally linear and nonlocal, as its coefficients depend on the larger-scale dynamics. It is also nonlocal in time, since SGS-turbulence generated earlier persists for some time. Developing an efficient bulk formula for air-sea drag, requires determining the functional form of: $C_{2D}\left(\sqrt{\langle \mathbf{u_s^2} \rangle}\right)$, as well as identifying the averaging scales, in both space and time.

In the experiments presented here, the turbulence is horizontally homogeneous, so the function C_{2D} has no spatial dependence. When the turbulent simulations are extended over longer durations, a statistically stationary state is reached, and the friction coefficient converges to a time-independent function. Ongoing work aims to estimate the function $C_{2D}\left(\sqrt{\langle \mathbf{u_s^2} \rangle}\right)$ in a homogeneous and stationary framework, as well as its dependence on the parameters, by continuing the simulations used in this study.

Code availability. The code can be obtained from the author upon request

Data availability. No data used

Appendix A: Stationarity of the shear mode

If the forcing $F(x)$ is in the y-direction and does only depend on the x-direction, and ignoring the non-linear term and neglecting the explicit viscosity in the atmosphere and the ocean, Eqs. 12 and 13 simplify to:

$$m_a \partial_t q_a = -\partial_x \left[C(\tilde{v})\tilde{v} \right] + F_q \tag{A1}$$

$$m_o \partial_t q_o = \partial_x \left[C(\tilde{v})\tilde{v} \right], \tag{A2}$$

https://doi.org/10.5194/egusphere-2026-5130
Preprint. Discussion started: 14 September 2026

where $F_q = \partial_x F$ is the vorticity of the forcing and $\tilde{v} = v_a - v_o$ is the y-component of the shear velocity. The latter becomes independent in time $\partial_t \tilde{v} = 0$, after a fast initial adjustment. This implies that $\partial_{tx}(\Psi_a - \Psi_o) = 0$, but note that $\partial_t(q_a - q_o) \neq 0$. We therefore get:

$$\partial_t(q_a - q_o) = \partial_t(-R_a^{-2}\Psi_a + R_o^{-2}\Psi_o) = -\partial_t\left[(R_a^{-2} + R_o^{-2})\Psi_a\right] = -(\frac{1}{m_a} + \frac{1}{m_o})\partial_x\left[C(\tilde{v})\tilde{v}\right] + \frac{F_q}{m_a} \quad \text{(A3)}$$

$$\partial_t(R_o^{-2}q_a - R_a^{-2}q_o) = \partial_t(R_o^{-2}\partial_{xx}\Psi_a - R_a^{-2}\partial_{xx}\Psi_o) = \partial_t\left[(R_o^{-2} + R_a^{-2})\partial_{xx}\Psi_a\right] = -(\frac{R_o^{-2}}{m_a} + \frac{R_a^{-2}}{m_o})\partial_x\left[C(\tilde{v})\tilde{v}\right] + \frac{R_o^{-2}}{m_a}F_q \quad \text{(A4)}$$

Applying the second derivative in x to Eq. A3 and introducing it in Eq. A4 gives:

$$(\frac{1}{m_a} + \frac{1}{m_o})\partial_{xxx}\left[C(\tilde{v})\tilde{v}\right] - \frac{\partial_{xx}F_q}{m_a} = -(\frac{R_o^{-2}}{m_a} + \frac{R_a^{-2}}{m_o})\partial_x\left[C(\tilde{v})\tilde{v}\right] + \frac{R_o^{-2}}{m_a}F_q \quad \text{(A5)}$$

$$(\frac{1}{m_a} + \frac{1}{m_o})\partial_{xxx}\left[C(\tilde{v})\tilde{v}\right] + (\frac{R_o^{-2}}{m_a} + \frac{R_a^{-2}}{m_o})\partial_x\left[C(\tilde{v})\tilde{v}\right] = \frac{R_o^{-2}}{m_a}F_q + \frac{\partial_{xx}F_q}{m_a}. \quad \text{(A6)}$$

When the forcing is monochromatic, as in the present case, $F = \hat{F}\sin(x/R)$ so is its vorticity $F_q = \frac{\hat{F}}{R}\cos(x/R)$. Integrating Eq. A6 in x gives:

$$(\frac{1}{m_a} + \frac{1}{m_o})\partial_{xx}\tilde{C} + (\frac{R_o^{-2}}{m_a} + \frac{R_a^{-2}}{m_o})\tilde{C} = \frac{R_o^{-2} - R^{-2}}{m_a}F, \quad \text{(A7)}$$

where $\tilde{C} = [C(\tilde{v})\tilde{v}]$. This leads to:

$$\tilde{C} = \alpha F \quad \text{with} \quad \alpha = \left[1 + \frac{m_a(R_a^{-2} - R^{-2})}{m_o(R_o^{-2} - R^{-2})}\right]^{-1}. \quad \text{(A8)}$$

Note that here we have the special case $R = R_a$ and therefore $\alpha = 1$. The second step consists in finding $C(\tilde{v})$ for the calculated $\tilde{C}$ and $\tilde{v}$, which is obtained from averaging the numerical simulations results. When we make the Ansatz of a linear Rayleigh drag, $C = \bar{a}$, then

$$\bar{a} = \frac{\alpha F}{\tilde{v}}. \quad \text{(A9)}$$

When we make the Ansatz of the extended quadratic drag-law, $C = \sqrt{(\bar{c}\tilde{v}(x))^2 + \bar{a}^2}$ then:

$$\bar{c}^2\tilde{v}(x)^4 + \bar{a}^2\tilde{v}(x)^2 = (\alpha F)^2 \quad \text{(A10)}$$

$$\bar{c}^2\partial_{xx}(\tilde{v}(x)^4) + \bar{a}^2\partial_{xx}(\tilde{v}(x)^2) = \partial_{xx}((\alpha F)^2). \quad \text{(A11)}$$

We know the forcing $F(x)$ in the experiment and $\tilde{v}(x)$ is obtained from the numerical integration. Determining the drag law $C(\tilde{v})$, means adjusting the parameters $\bar{c}$ and $\bar{v}$ in $C(x) = \sqrt{(\bar{c}\tilde{v}(x))^2 + \bar{a}^2}$ so that $[C(x)\tilde{v}] = \tilde{C}(x)$, where $\tilde{C}(x)$ is obtained from Eq. A8.

When the forcing is $F(x) = \hat{F}\sin(x/R)$ then $F^2(x) = \frac{\hat{F}^2}{2}(1 - \cos(2x/R))$ we have $F(\pi R/2) = \hat{F}$, $\partial_x F^2(\pi R/2) = 0$ and $\partial_{xx}F^2(\pi R/2) = \frac{-2}{R^2}\hat{F}^2$. When Eqs. A10 and A11 are evaluated at $x = \pi R/2$, using the symbols $\hat{v}^2 = \tilde{v}^2(\pi R/2)$ and $\hat{v}^2_{xx} =$

https://doi.org/10.5194/egusphere-2026-5130
Preprint. Discussion started: 14 September 2026

$\partial_{xx}(\tilde{v}(\pi R/2))^2$, these equations form a linear system in $\bar{c}^2$ and $\bar{a}^2$:

$$\hat{v}^2\bar{c}^2 + \bar{a}^2 = \frac{(\alpha\hat{F})^2}{\hat{v}^2} \tag{A12}$$

$$2\hat{v}^2\bar{c}^2 + \bar{a}^2 = -\frac{2(\alpha\hat{F})^2}{R^2(\hat{v}^2_{xx})}, \tag{A13}$$

where I used $\partial_x\tilde{v}(R/4) = 0$. The solutions is:

$$\bar{c}^2 = -\left(\frac{\alpha\hat{F}}{\hat{v}}\right)^2\left[\frac{1}{\hat{v}^2} + \frac{2}{R^2\partial_{xx}(\hat{v}^2)}\right] \tag{A14}$$

$$\bar{a}^2 = (\alpha\hat{F})^2\left[\frac{2}{\hat{v}^2} + \frac{2}{R^2\partial_{xx}(\hat{v}^2)}\right]. \tag{A15}$$

The such calculated parameters are used to obtain the average velocity profile:

$$v_R = \frac{1}{\sqrt{2}\bar{c}}\sqrt{-\bar{a}^2 + \sqrt{\bar{a}^4 + 4\bar{c}^2F^2}} \tag{A16}$$

which can be compared to $\tilde{v}$ to evaluate the approximation, as done in Fig. 2.

Author contributions. work done by AW

Competing interests. no competing interest

Acknowledgements.

https://doi.org/10.5194/egusphere-2026-5130
Preprint. Discussion started: 14 September 2026

References

Alexander, M. A., Bladé, I., Newman, M., Lanzante, J. R., Lau, N.-C., and Scott, J. D.: The atmospheric bridge: The influence of ENSO teleconnections on air–sea interaction over the global oceans, Journal of Climate, 15, 2205–2231, 2002.

Arbic, B. K. and Scott, R. B.: On quadratic bottom drag, geostrophic turbulence, and oceanic mesoscale eddies, Journal of physical oceanography, 38, 84–103, 2008.

Bjerknes, J.: Atlantic air-sea interaction, in: Advances in geophysics, vol. 10, pp. 1–82, Elsevier, 1964.

Boffetta, G. and Ecke, R. E.: Two-dimensional turbulence, Annual Review of Fluid Mechanics, 44, 427–451, 2012.

Buijsman, M. C., Ansong, J. K., Arbic, B. K., Richman, J. G., Shriver, J. F., Timko, P. G., Wallcraft, A. J., Whalen, C. B., and Zhao, Z.: Impact of parameterized internal wave drag on the semidiurnal energy balance in a global ocean circulation model, Journal of Physical Oceanography, 46, 1399–1419, 2016.

Castellari, S., Pinardi, N., and Leaman, K.: A model study of air–sea interactions in the Mediterranean Sea, Journal of Marine Systems, 18, 89–114, 1998.

Csanady, G. T.: Air-sea interaction: laws and mechanisms, Cambridge University Press, 2001.

Deardorff, J. W.: Parameterization of the planetary boundary layer for use in general circulation models, Monthly Weather Review, 100, 93–106, 1972.

Emanuel, K. A.: An air-sea interaction theory for tropical cyclones. Part I: Steady-state maintenance, Journal of the Atmospheric Sciences, 43, 585–605, 1986.

Fairall, C. W., Bradley, E. F., Rogers, D. P., Edson, J. B., and Young, G. S.: Bulk parameterization of air-sea fluxes for tropical ocean-global atmosphere coupled-ocean atmosphere response experiment, Journal of Geophysical Research: Oceans, 101, 3747–3764, 1996.

Kondo, J.: Air-sea bulk transfer coefficients in diabatic conditions, Boundary-Layer Meteorology, 9, 91–112, 1975.

Lott, F., Beljaars, A., and Deremble, B.: Suggestions for unifying the parametrizations of turbulent orographic form drag, mountain wave drag, and flow blocking, Quarterly Journal of the Royal Meteorological Society, p. e70169, 2026.

Melville, W. K.: The role of surface-wave breaking in air-sea interaction, Annual review of fluid mechanics, 28, 279–321, 1996.

Moulin, A. and Wirth, A.: A drag-induced barotropic instability in air–sea interaction, Journal of Physical Oceanography, 44, 733–741, 2014.

Moulin, A. and Wirth, A.: Momentum Transfer Between an Atmospheric and an Oceanic Layer at the Synoptic and the Mesoscale: An Idealized Numerical Study, Boundary-Layer Meteorology, 160, 551–568, 2016.

Pelletier, C., Lemarié, F., Blayo, E., Bouin, M.-N., and Redelsperger, J.-L.: Two-sided turbulent surface-layer parameterizations for computing air–sea fluxes, Quarterly Journal of the Royal Meteorological Society, 147, 1726–1751, 2021.

Pond, S. and Bryan, K.: Numerical models of the ocean circulation, Reviews of geophysics, 14, 243–263, 1976.

Schlichting, H. and Gersten, K.: Boundary-layer theory, springer, 2016.

Small, R. d., DeSzoeke, S., Xie, S., O'neill, L., Seo, H., Song, Q., Cornillon, P., Spall, M., and Minobe, S.: Air–sea interaction over ocean fronts and eddies, Dynamics of Atmospheres and Oceans, 45, 274–319, 2008.

Stevens, B., Duan, J., McWilliams, J. C., Münnich, M., and Neelin, J. D.: Entrainment, Rayleigh friction, and boundary layer winds over the tropical Pacific, Journal of climate, 15, 30–44, 2002.

Stocker, T. F., Qin, D., Plattner, G., Tignor, M., Allen, S., Boschung, J., Nauels, A., Xia, Y., Bex, V., and Midgley, P.: Climate change 2013: the physical science basis. Intergovernmental panel on climate change, working group I contribution to the IPCC fifth assessment report (AR5), New York, 2013.

https://doi.org/10.5194/egusphere-2026-5130
Preprint. Discussion started: 14 September 2026

Vallis, G. K.: Atmospheric and oceanic fluid dynamics, Cambridge University Press, 2017.

Van Westen, R. M., Kliphuis, M., and Dijkstra, H. A.: Physics-based early warning signal shows that AMOC is on tipping course, Science advances, 10, eadk1189, 2024.

Veron, F.: Ocean spray, Annual Review of Fluid Mechanics, 47, 507–538, 2015.

Wei, Z., Miyano, A., and Sugita, M.: Drag and bulk transfer coefficients over water surfaces in light winds, Boundary-layer meteorology, 160, 319–346, 2016.

Wirth, A.: Estimation of friction parameters in gravity currents by data assimilation in a model hierarchy, Ocean Science, 7, 245–255, 2011.

Wirth, A.: A fluctuation–dissipation relation for the ocean subject to turbulent atmospheric forcing, Journal of Physical Oceanography, 48, 831–843, 2018.

Wirth, A.: On fluctuating momentum exchange in idealised models of air–sea interaction, Nonlinear Processes in Geophysics, 26, 457–477, 2019.

Wu, L., Sahlée, E., Nilsson, E., and Rutgersson, A.: A review of surface swell waves and their role in air–sea interactions, Ocean Modelling, 190, 102 397, 2024.